Inertialess temporal and spatio-temporal stability analysis of the two-layer film flow with density stratification

J. Hu, S. Millet, V. Botton, H. Ben Hadid, and D. Henry[a)]
Laboratoire de Mécanique des Fluides et d'Acoustique, UMR CNRS 5509, Ecole Centrale de Lyon/ Université Claude Bernard Lyon 1/INSA de Lyon, ECL, 36 Avenue Guy de Collongue, 69134 Ecully Cedex, France

(Received 16 September 2005; accepted 15 August 2006; published online 2 October 2006)

This paper presents a temporal, spatial, and spatio-temporal linear stability analysis of the two-layer film flow down a plate tilted at an angle θ. It is based on a zero Reynolds number approximation to the Orr-Sommerfeld equations and a zero surface tension approximation to both surface boundary conditions. The combined effects of density and viscosity stratifications are systematically investigated. The subtle influence of density stratification is first put into light by a temporal analysis for $\theta=0.2$; when increasing/decreasing the density ratio (upper fluid/lower fluid), the two-layer film flow becomes much more unstable/stable with respect to the finite wavelength instability. Moreover, below a critical density ratio this finite wavelength instability even disappears, whatever the viscous ratio. Concerning the long wave instability, it becomes dominant when decreasing the density ratio below 1 and is even triggered in a region which was stable for equal density layers. The spatio-temporal analysis shows that the instability is convective for incline angles that are not too small as $\theta=0.2$. The study of the local growth rates of the spatio-temporal instability as a function of the ray velocity V shows that there is a transition between long wave and short wave instabilities which has been determined by using the Briggs-Bers collision criterion. Accordingly, there exists a jump for the local oscillatory frequency, spatial amplification rate, and spatial wave number due to this transition. Due to the existence of the absolute Rayleigh-Taylor instability for $\theta=0$, the transition from convective to absolute instability can be detected for values of θ smaller than 0.2, and absolute/convective instability boundary curves have been obtained for varying characteristic parameters. © *2006 American Institute of Physics*. [DOI: 10.1063/1.2357026]

I. INTRODUCTION

A one-layer liquid film flowing down an inclined plane is one of the most important models used to study the dynamical behaviors of open flows, such as surface waves, solitary waves, and transitions from laminar flow to turbulence, for its technological relevance, conceptual simplicity, and rich dynamical phenomenology.[1] However, in many industrial processes, multilayered systems are usually used, such as the coating of a color film which sometimes consists of more than ten different layers. Multilayer flow can also be useful to model some environmental flows, such as rock glaciers mentioned by Loewenherz and Lawrence.[2] It is thus significant and important to explore the dynamical characteristics of multilayered liquid films.

Kao[3–5] first investigated the long wave instability of two-layer falling films with different heights, different densities, and different viscosities. By using the same long wave approximation as Yih's[6] for one-layer films, he obtained two critical Reynolds numbers and identified them to correspond to two modes of instabilities, now usually regarded as the surface mode and the interface mode, respectively. The surface mode always has a faster phase velocity than the interface mode in the long wave approximation. When the less viscous layer is adjacent to the plate, the interfacial instability occurs below a critical Reynolds number, i.e., the interface mode exists even when the Reynolds number approaches zero. Due to the inertialess character of the destabilization, the interface mode has also been termed as inertialess instability. Later, Loewenherz and Lawrence[2] studied the inertialess instability through a zero Reynolds number approximation to the Orr-Sommerfeld equations. They focused on the role of viscosity stratification, assuming equal density in the two layers. Their curves of temporal growth rates with different wave numbers for zero surface tension showed that the inertialess instability can occur at finite wavelength. Furthermore, a detailed linear instability analysis by Chen[7] verified that the unstable wave motion can occur when the less viscous layer is in the region next to the wall for any Reynolds number and any finite interface and surface tension. By use of a kinetic energy budget, Jiang *et al.*[8] revealed that the work done by the shear stress at the unperturbed free surface is essential to cause the inertialess instability.

The absolute and convective instability for a single-layer falling film has been studied intensively by Brevdo *et al.*[9] They focused on the full linearized Navier-Stokes equations to investigate the characteristics of the absolute and convective instability through the exact Briggs-Bers collision criterion. They explored a large region of the parameter space and pointed out that the one-layer film flow is convectively un-

[a)]Author to whom correspondence should be addressed. Electronic mail: Daniel.Henry@ec-lyon.fr

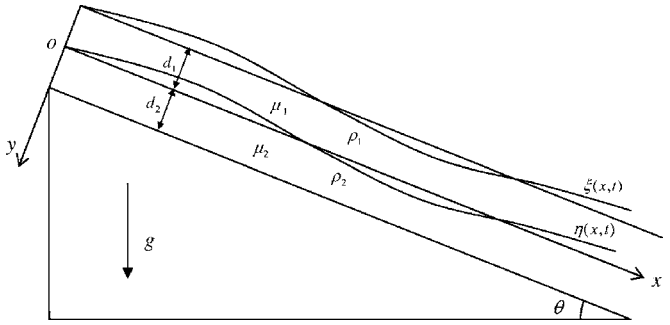

FIG. 1. Sketch map of the two layer film flow along an inclined plate.

stable, which agrees with all done experiments. Considering the convective property of such open flows, they further studied the properties of the spatially amplifying waves and found results in complete agreement with the experiments performed by Liu *et al.*[10] Yet such a study about the absolute or convective nature of the instability has never been made for multilayer film flows. It is performed in the present paper in the case of the inertialess instability of two-layer film flows.

Our inertialess interfacial instability analysis is performed under the same zero Reynolds number approximation as Loewenherz and Lawrence,[2] and without considering any surface tension effects; the formulation of the problem with these assumptions is recalled in Sec. II. The present paper focuses on the density stratification effect, which has received less attention in the past than viscosity stratification. We consider in detail these effects through a linear temporal approach in Sec. III. We then study the spatio-temporal nature (absolute or convective) of the instability of the two-layer film flow in Secs. IV and V. Our results show that the two-layer film flow with zero Reynolds number and zero surface tension is convectively unstable for $\theta=0.2$ in a region of physical parameters corresponding to various density and viscous ratios. But for smaller incline angles, absolute/convective instability boundary curves have been detected. Finally, Sec. VI is devoted to the study of the properties of the spatially amplifying waves in the region of parameters where the instability is convective.

II. FORMULATION OF THE STABILITY PROBLEM

We consider a two-dimensional gravity-driven laminar flow of two liquid layers down an inclined flat plate tilted at an angle θ to the horizontal (Fig. 1). The two liquid layers have different thicknesses d_i, densities ρ_i, and dynamical viscosities μ_i (subscript $i=1,2$ denotes the upper and lower fluids, respectively). The gas above the two layers is assumed to be passive, and both surface tensions on the free surface between the gas and the upper layer and on the interface between the two layers are neglected. Driven by the component $g\sin\theta$ of gravity along the plate, the dimensionless basic streamwise velocity solutions of the Navier-Stokes equations are given by

$$U_1(y)=a_1y^2+b_1y+c_1, \quad -\delta\le y\le 0, \tag{2.1a}$$

$$U_2(y)=a_2y^2+b_2y+c_2, \quad 0\le y\le 1, \tag{2.1b}$$

in which $a_1=-\gamma K/2m$, $a_2=-K/2$, $b_1=-\gamma\delta K/m$, $b_2=-\gamma\delta K$, $c_1=c_2=K/2+\gamma\delta K$, where δ, γ and m, respectively, represent the ratios of depths, densities, and dynamical viscosities

$$\delta=\frac{d_1}{d_2}, \quad \gamma=\frac{\rho_1}{\rho_2}, \quad m=\frac{\mu_1}{\mu_2}, \tag{2.2}$$

and $K=(1+\delta)[1/3+\delta/2+\gamma(\delta/2+\delta^2+\delta^3/3m)]^{-1}$. Following Kao,[5] the characteristic length is chosen to be the lower layer thickness d_2 and the characteristic velocity is the mean velocity obtained by integration over the two-layer thickness, $U_a=\rho_2gd_2^2\sin\theta/\mu_2K$. The Reynolds numbers and Froude number are now defined as

$$R_1=\frac{\rho_1U_ad_2}{\mu_1}, \quad R_2=\frac{\rho_2U_ad_2}{\mu_2}, \quad F=\frac{U_a}{(gd_2)^{1/2}}. \tag{2.3}$$

It then follows that $R_1=\gamma R_2/m$ and $KF^2=R_2\sin\theta$.

Induced by the component $g\cos\theta$ of gravity, the dimensionless basic hydrostatic pressures are represented as

$$P_1=\frac{\cos\theta}{F^2}(y+\delta), \quad -\delta\le y\le 0, \tag{2.4a}$$

$$P_2=\frac{\cos\theta}{F^2}(y+\gamma\delta), \quad 0\le y\le 1, \tag{2.4b}$$

where P_1 and P_2 are normalized by $\rho_1U_a^2$ and $\rho_2U_a^2$, respectively. Thus, at the undisturbed interface $y=0$, the equality of pressure yields $\gamma P_1=P_2$.

The disturbed flow can be decomposed into $u_i=U_i+u_i'$, $v_i=v_i'$, $p_i=P_i+p_i'$. ξ and η denote small departures from the free surface and interface position, respectively. Then the linearized governing equations are expressed as

$$\frac{\partial u_i'}{\partial x}+\frac{\partial v_i'}{\partial y}=0, \tag{2.5a}$$

$$\frac{\partial u_i'}{\partial t}+U_i\frac{\partial u_i'}{\partial x}+\frac{dU_i}{dy}v_i'=-\frac{\partial p_i'}{\partial x}+\frac{1}{R_i}\Delta u_i', \tag{2.5b}$$

$$\frac{\partial v_i'}{\partial t}+U_i\frac{\partial v_i'}{\partial x}=-\frac{\partial p_i'}{\partial y}+\frac{1}{R_i}\Delta v_i', \tag{2.5c}$$

where $\Delta=\partial^2/\partial x^2+\partial^2\partial y^2$. The linearized boundary conditions correspond to one kinematic and two dynamical boundary conditions along both the free surface and the interface, and to no-slip and no-penetration boundary conditions along both the interface and the inclined wall:

$$\frac{\partial\xi}{\partial t}+U_1\frac{\partial\xi}{\partial x}=v_1', \quad \text{at } y=-\delta, \tag{2.6a}$$

$$\frac{\partial u_1'}{\partial y}+\frac{\partial v_1'}{\partial x}+\frac{d^2U_1}{dy^2}\xi=0, \quad \text{at } y=-\delta, \tag{2.6b}$$

$$\gamma p_1' + \gamma \frac{dP_1}{dy}\xi + \frac{2\gamma}{R_1}\frac{\partial u_1'}{\partial x} = 0, \quad \text{at } y = -\delta, \tag{2.6c}$$

$$\frac{\partial \eta}{\partial t} + U_1 \frac{\partial \eta}{\partial x} = v_1', \quad \text{at } y = 0, \tag{2.6d}$$

$$m\left(\frac{\partial u_1'}{\partial y} + \frac{\partial v_1'}{\partial x} + \frac{d^2U_1}{dy^2}\eta\right) = \left(\frac{\partial u_2'}{\partial y} + \frac{\partial v_2'}{\partial x} + \frac{d^2U_2}{dy^2}\eta\right),$$

$$\text{at } y = 0, \tag{2.6e}$$

$$\gamma p_1' + \gamma \frac{dP_1}{dy}\eta + \frac{2\gamma}{R_1}\frac{\partial u_1'}{\partial x} = p_2' + \frac{dP_2}{dy}\eta + \frac{2}{R_2}\frac{\partial u_2'}{\partial x},$$

$$\text{at } y = 0, \tag{2.6f}$$

$$u_1' - u_2' = \left(\frac{dU_2}{dy} - \frac{dU_1}{dy}\right)\eta, \quad \text{at } y = 0, \tag{2.6g}$$

$$v_1' = v_2', \quad \text{at } y = 0, \tag{2.6h}$$

$$u_2' = v_2' = 0, \quad \text{at } y = 1. \tag{2.6i}$$

Now, we assume that there are normal mode solutions of the form

$$u_i'(y,x,t) = \hat{u}_i(y)e^{i(kx-\omega t)}, \quad v_i'(y,x,t) = \hat{v}_i(y)e^{i(kx-\omega t)},$$

$$p_i'(y,x,t) = \hat{p}_i(y)e^{i(kx-\omega t)},$$

$$\xi = \hat{\xi}e^{i(kx-\omega t)}, \quad \eta = \hat{\eta}e^{i(kx-\omega t)}.$$

Substituting them into the disturbed linearized governing equations and the corresponding boundary conditions, then eliminating the disturbed pressure p' and disturbed streamwise velocity u', yields the linear stability equations (Orr-Sommerfeld equations) for the two fluids,

$$(D^2 - k^2)^2\hat{v}_i = iR_i[(U_ik - \omega)(D^2 - k^2) - D^2U_ik]\hat{v}_i, \tag{2.7}$$

where $D = d/dy$.

The linear boundary conditions at the free surface, the interface and the plate wall become:

$$i[U_1k - \omega]\hat{\xi} = \hat{v}_1, \quad \text{at } y = -\delta, \tag{2.8a}$$

$$(D^2 + k^2)\hat{v}_1 - iD^2U_1k\hat{\xi} = 0, \quad \text{at } y = -\delta, \tag{2.8b}$$

$$m[D^2 - 3k^2 - iR_1(U_1k - \omega)]D\hat{v}_1 + \gamma K \cot\theta k^2\hat{\xi} = 0,$$

$$\text{at } y = -\delta, \tag{2.8c}$$

$$i[U_2k - \omega]\hat{\eta} = \hat{v}_2, \quad \text{at } y = 0, \tag{2.8d}$$

$$m[(D^2 + k^2)\hat{v}_1 - iD^2U_1k\hat{\eta}] = (D^2 + k^2)\hat{v}_2 - iD^2U_2k\hat{\eta},$$

$$\text{at } y = 0, \tag{2.8e}$$

$$m[D^2 - 3k^2 - iR_1(U_1k - \omega)]D\hat{v}_1 - [D^2 - 3k^2 - iR_2(U_2k - \omega)]D\hat{v}_2 + i(\gamma DU_1 - DU_2)R_2k\hat{v}_1 + [(\gamma - 1)K\cot\theta]k^2\hat{\eta} = 0,$$

$$\text{at } y = 0, \tag{2.8f}$$

$$D\hat{v}_1 - D\hat{v}_2 = ik(DU_1 - DU_2)\hat{\eta}, \quad \text{at } y = 0, \tag{2.8g}$$

$$\hat{v}_1 = \hat{v}_2, \quad \text{at } y = 0, \tag{2.8h}$$

$$\hat{v}_2 = D\hat{v}_2 = 0, \quad \text{at } y = 1. \tag{2.8i}$$

Our definitions for the coordinates and dimensionless parameters are the same as those of Kao.[5]

The two Orr-Sommerfeld (O-S) equations are ordinary differential equations in terms of $\hat{v}_i$ and can be regarded as a two-point boundary value problem. If there exists a nontrivial solution for the equations, a corresponding dispersion relation $D(k,\omega;R_2,\delta,\gamma,m,\theta)=0$ should be satisfied, and an eigenvalue problem has to be solved.

As the interface instability even occurs at low Reynolds numbers, it is interesting to first study the inertialess stability and let the Reynolds number be zero. Thus the linear instability equations, i.e., the O-S equations (2.7), can be reduced to

$$(D^2 - k^2)^2\hat{v}_i = 0. \tag{2.9}$$

Obviously, these two equations have general solutions of the form

$$\hat{v}_1 = A_1e^{ky} + B_1e^{-ky} + C_1ye^{ky} + D_1ye^{-ky}, \tag{2.10a}$$

$$\hat{v}_2 = A_2e^{ky} + B_2e^{-ky} + C_2ye^{ky} + D_2ye^{-ky}. \tag{2.10b}$$

Substituting them into the corresponding linear boundary conditions (2.8) with the Reynolds numbers set to zero, one obtains a system of ten homogeneous algebraic equations in the ten unknowns $\hat{\xi}, \hat{\eta}, A_1, B_1, C_1, D_1, A_2, B_2, C_2, D_2$, given below:

$$\begin{bmatrix}
i[U_1(-\delta)k-\omega] & 0 & -e^{-k\delta} & -e^{k\delta} & \delta e^{-k\delta} & \delta e^{k\delta} & 0 & 0 & 0 & 0 \\
-iD^2U_1(-\delta)k & 0 & 2k^2e^{-k\delta} & 2k^2e^{k\delta} & 2(k-\delta k^2)e^{-k\delta} & -2(k+\delta k^2)e^{k\delta} & 0 & 0 & 0 & 0 \\
\gamma K\cot\theta k^2 & 0 & -2mk^3e^{-k\delta} & 2mk^3e^{k\delta} & 2m\delta k^3e^{-k\delta} & -2m\delta k^3e^{k\delta} & 0 & 0 & 0 & 0 \\
0 & 0 & 1 & 1 & 0 & 0 & -1 & -1 & 0 & 0 \\
0 & ik[DU_2(0)-DU_1(0)] & k & -k & 1 & 1 & -k & k & -1 & -1 \\
0 & i[U_2(0)k-\omega] & 0 & 0 & 0 & 0 & -1 & -1 & 0 & 0 \\
0 & i[D^2U_2(0)-mD^2U_1(0)]k & 2mk^2 & 2mk^2 & 2mk & -2mk & -2k^2 & -2k^2 & -2k & 2k \\
0 & (\gamma-1)K\cot\theta k^2 & -2mk^3 & 2mk^3 & 0 & 0 & 2k^3 & -2k^3 & 0 & 0 \\
0 & 0 & 0 & 0 & 0 & 0 & e^k & e^{-k} & e^k & e^{-k} \\
0 & 0 & 0 & 0 & 0 & 0 & ke^k & -ke^{-k} & (1+k)e^k & (1-k)e^{-k}
\end{bmatrix}
\begin{bmatrix}
\hat{\xi} \\ \hat{\eta} \\ A_1 \\ B_1 \\ C_1 \\ D_1 \\ A_2 \\ B_2 \\ C_2 \\ D_2
\end{bmatrix} = 0$$

It is well known that such a system admits solutions if and only if the corresponding 10×10 determinant is zero. We thus obtain an analytical dispersion relation which can be represented as

$$\alpha\omega^2+\beta\omega+\chi=0, \tag{2.11}$$

where the coefficients α, β, and χ are given in the Appendix. As Loewenherz and Lawrence[2] have pointed out, the two roots resulting from the dispersion relation (2.11) correspond to the surface mode and the interface mode, respectively. They have also found that the surface mode is always linearly stable. Our study will then focus on the inertialess interfacial instability.

III. TEMPORAL INSTABILITY

Loewenherz and Lawrence[2] have already studied the inertialess temporal instability of two-layer liquid films down an inclined plane. They mainly investigated the effect of viscosity stratification with the restriction to the case of zero-Reynolds number, zero interfacial and surface tensions, and matched density. Under this restriction, they found that when the less viscous layer is adjacent to the wall, the flow is unstable in a large domain ranging from long wave to short wave instabilities. Especially, they pointed out that the maximum growth rate occurs at a finite wavelength comparable to the total depth of the layered system. Later, Chen[7] extended the same problem by considering low-Reynolds numbers and nonzero interfacial and surface tensions, but still matched density. It is shown from his linear stability analysis that the flow is always unstable with the onset of wavy motions when the less viscous layer is in the region next to the wall for any Reynolds number and any finite interface and surface tensions. From these works, it may be seen that the effect of density stratification is not yet studied, although Kao[3] has identified that for any finite Reynolds number the two-layer flow is more stable or unstable than the homogeneous case of equal total depth, depending on whether the upper layer is lighter or heavier than the lower layer. In this section, we investigate the effect of density stratification for the two layer liquid films with the same restrictions as Loewenherz and Lawrence,[2] namely zero-Reynolds number and zero interfacial and surface tensions, and the same inclination of the plate, i.e. $\theta=0.2$.

The results of our linear stability analysis have been first validated by comparison with the growth rates shown in Figs. 3 and 4 of Chen[7] for $\gamma=1$, $m=2.5$, $\theta=0.2$, and different depth ratios δ. The agreement is so good that our curves could not be distinguished from Chen's curves.

To show the effect of the density stratification, we plot, in Fig. 2, neutral curves of temporal instability in the $m-k$ parameter space for different density ratios γ and for equal thickness of the two layers ($\delta=1$). For a good understanding of these figures, note that for each referenced value of γ, the neutral curves give the transition between stable and unstable regions. These regions and their stability can be clearly identified for a given value of γ by putting aside the neutral curves corresponding to other values of γ. When $\gamma=1$ and $m=1$, the two-layer model degenerates into a homogeneous single layer model (for this case, the depth ratio loses any physical meaning since no interface exists). The $m=1$ line is then a neutral curve for $\gamma=1$, as already identified by Loewenherz and Lawrence.[2] As may be seen from Fig. 2, for $\gamma=1$ the $m=1$ line delimits a stable domain for $m\leq1$ and a domain for $m>1$ which is unstable at all wave numbers, except for large viscous ratios m where a stable zone exists at intermediate wave numbers. In the following, we will comment on the effect of density stratification ($\gamma\neq1$).

• For $\gamma\geq1$ (which corresponds to the denser fluid in the upper layer), from Figs. 2(a) and 2(b), we see globally an enlargement of the unstable region with the increase of γ:

-The region $m<1$ which was stable for $\gamma=1$, becomes unstable for $\gamma\geq1$ beyond a cutoff wave number [Fig. 2(a)] depending on γ and m. More precisely, the neutral curves in this domain intersect each other near $m=1$ at an almost fixed point, determining an enlargement of the unstable wave number region as the density ratio γ and the viscous ratio m increase. The maximum growth rate of the instability occurring in this domain corresponds to finite wave numbers (between 2 and 4), the intensity of the peak increasing and its position moving to smaller wave numbers as γ and m increase.

-The neutral curves for $\gamma\geq1$ shown in Fig. 2(a) also exist for $m>1$, but in a very small long wave region. They delimit a small stable long wave domain close to $m=1$, which vanishes as γ decreases to 1.

-For m values beyond this stable long wave domain, there is a region where the flow is unstable at all wave num-

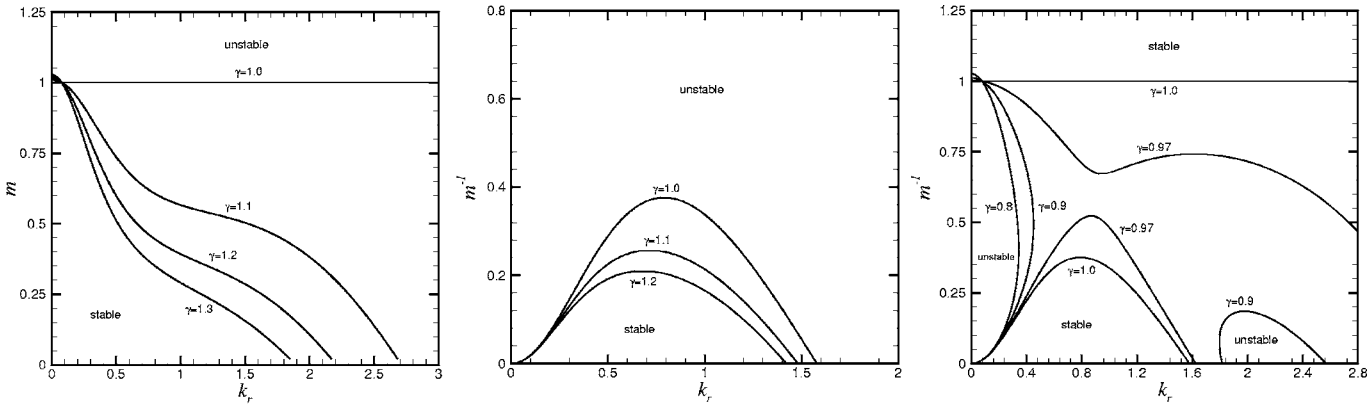

FIG. 2. Neutral curves of the inertialess interfacial instability for different density ratios γ in the $m-k$ parameter space for $\delta=1.0$ and $\theta=0.2$.

bers [shown in Fig. 2(b) for $m>1.25$]. This region increases in size as γ increases, in connection with the decrease of the stable zone at large m. As may be seen from the growth-rates in Figs. 3(a) ($m=2.5$) and 3(b) ($\gamma=1$), the maximum growth-rate in this domain occurs around $k_r=2$, but for large m a second small peak appears at small wave numbers, separated from the main peak by the stable zone.

• For $\gamma<1$ (which corresponds to the lighter fluid in the upper layer) [Fig. 2(c)], there is rather a decrease of the unstable region with the decrease of γ:

-Note first that the domain with $\gamma<1$ and $m<0.8$, not shown in Fig. 2(c), remains stable.

-From Fig. 2(c), it may be seen that the neutral curves form a saddle-like structure around $\gamma=0.97$. Such a structure shows that the unstable region becomes smaller and is associated with smaller maximum growth-rates when decreasing the density ratio [see also Fig. 3(a)]. The long wave unstable region (which persists when γ decreases) has its largest extent in terms of the wave number at moderate viscous ratios near $1/m=0.5$, i.e., $m=2$, and, as may be seen in Fig. 3(b), the maximum growth-rate for this long wave instability rises to a maximum in the same range of viscous ratios. A similar variation of the growth-rate is observed in Fig. 3(b) for the finite wavelength instability.

-The neutral curves at long wavelength for $\gamma<1$ [shown in Fig. 2(c)] also exist for $m>1$, but in a very small long wave region. They delimit for $\gamma<1$ a small unstable long wave domain close to $m=1$ where the long wavelength instability should be triggered.

-The finite wavelength unstable region, which may be seen for a density ratio $\gamma=0.9$ around $k_r=2$ in Fig. 2(c), vanishes when decreasing the density ratio down to 0.8. This implies that there is a critical density ratio below which the finite wavelength instability disappears, whatever the viscous

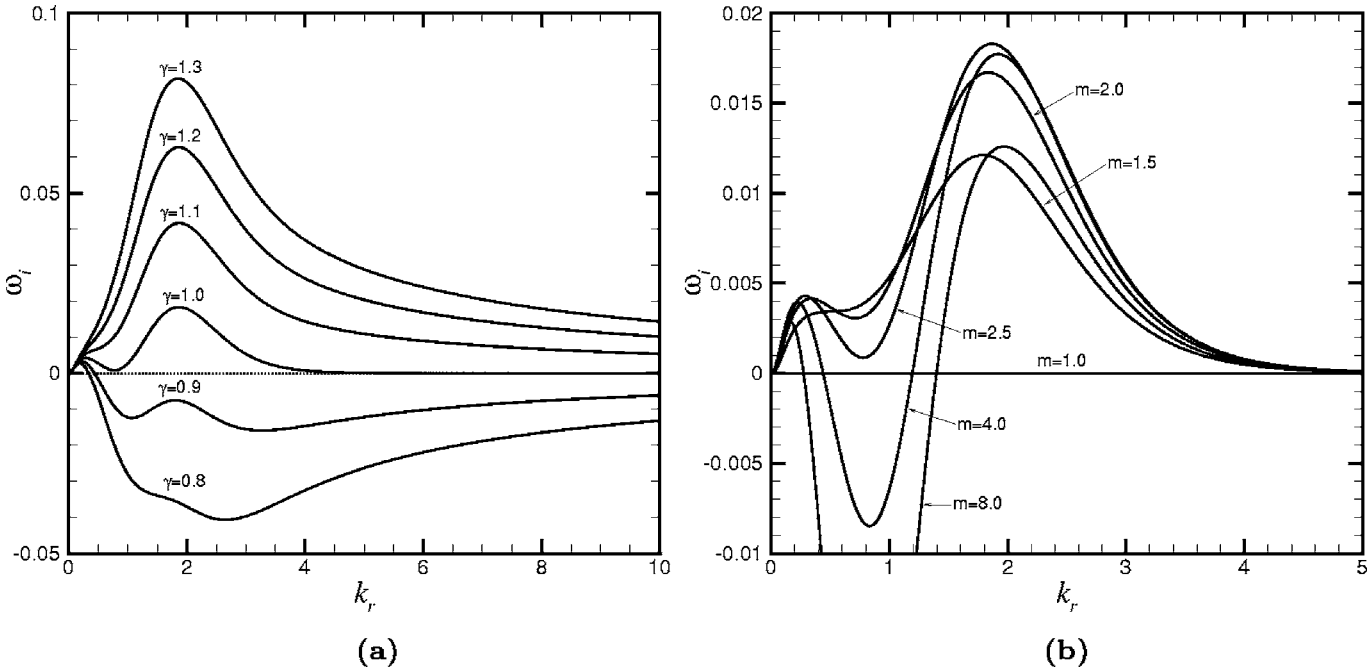

FIG. 3. Growth rates of the inertialess interfacial instability for (a) $m=2.5$ and different density ratios γ, and (b) $\gamma=1.0$ and different viscous ratios m ($\delta=1$ and $\theta=0.2$).

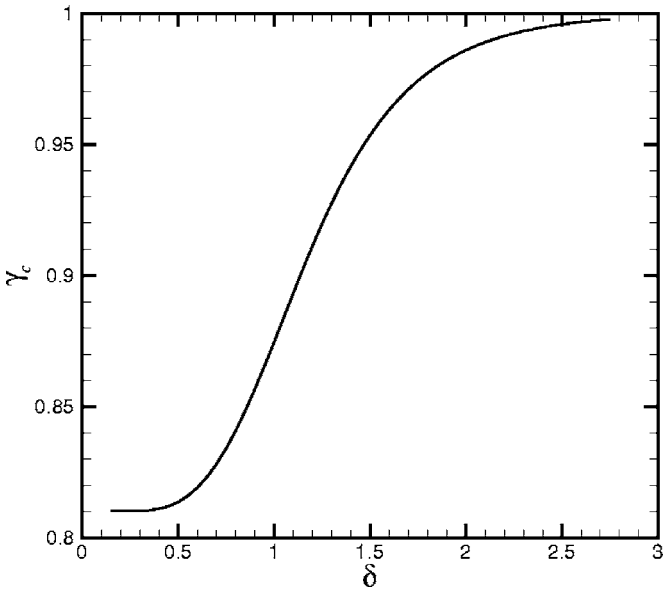

FIG. 4. Critical density ratios given as a function of the depth ratio and indicating the limit below which there does not exist finite wavelength interfacial instability for any large viscous ratio. The incline angle is $\theta=0.2$.

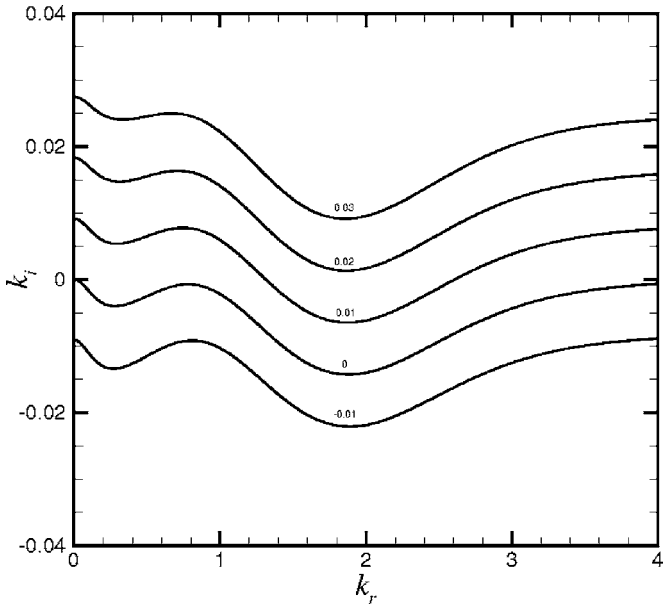

FIG. 5. Deformation of the spatial branches $k_n(\omega)$ for decreasing growth rates ω_i from 0.03 to −0.01 for the case $m=2.5$, $\gamma=1$, $\delta=1$ and $\theta=0.2$.

ratio. In order to verify this implication, we have computed the neutral curve in the $\gamma-k$ parameter space for $\gamma<1$ and $m=400$, and found that this curve effectively presents a minimum. This minimum has been checked to be nearly invariant for a viscous ratio above $m=400$ and can then be considered as the critical density ratio. Through such a process, we have plotted in Fig. 4 the critical density ratio for different depth ratios δ. This critical density ratio increases from about 0.81 for very small depth ratios to nearly 1 for depth ratios of the order of 3 or greater. The disappearance of the finite wavelength instability has consequences which contrast with Chen's results[7] obtained for $\gamma=1$; he showed indeed that for $\delta<2$, the finite wave peak dominates; this does not hold anymore if sufficient density stratification is present ($\gamma<1$) as this peak will disappear and the long wave instability will then be dominant.

From the above linear stability analysis, we found that the larger the density ratio γ, the more unstable the two-layer film flow, in particular with the situation for $\gamma>1$ (inverse density stratification) being unstable for any viscous ratio m. This behavior is in fact valid for the whole parameter space, except for a very small parameter region near $m=1$ and $k_r=0$ where, unexpectedly, it is observed that the decrease of γ below 1 (normal density stratification) induces instability [see Fig. 2(c)]. Our linear stability analysis also shows that the largest maximum growth-rate for long wave instabilities (rather dominant in the unstable domain for $\gamma<1$) as well as for finite wavelength instabilities (dominant for $\gamma>1$) occurs at some moderate viscous ratio. Finally, for the finite wavelength instability, when the density ratio γ (less than one) is less than a critical value, this instability does not appear any more within that region. From these results, we can see that the density stratification has some remarkable effects on the linear instability of inertialess two-layer film flows.

IV. SPATIO-TEMPORAL INSTABILITY

Basically, when an amplifying wave packet is convected away from its local position, the wave packet would be said to be convectively unstable.[11–14] If otherwise the amplification can be observed locally, the wave packet would be said to be absolutely unstable. Generally, the absolute/convective nature of the instability is determined by the sign of the absolute growth rate $\omega_{oi}=\mathrm{Im}[\omega(k_0)]$ defined at the saddle point k_0 of the dispersion relation, i.e., when $\frac{d\omega}{dk}|_{k_0}=0$. In these expressions, k is a complex wave number and ω is a complex frequency. If the absolute growth rate ω_{0i} is greater than zero (lower than zero), the flow is said to be absolutely (convectively) unstable. But it should be noticed that the saddle point k_0 used to identify AI/CI must satisfy the Briggs-Bers collision criterion, i.e., the saddle point must be a pinch point produced by two distinct spatial branches of solutions of the dispersion relation, $k_n^{\pm}(\omega)$, coming, respectively, from the upper and lower half k planes, and commonly referred to as upstream and downstream branches.

In fact, the determination of AI/CI can be done by a pinching process, i.e., by following the deformation of the spatial branches in the complex k plane as the temporal growth rate ω_i is decreased from its maximum value to zero. If under such a process there is a collision of two spatial branches $k_n^{\pm}(\omega)$ coming from opposite sides of the real k axis, i.e., the Briggs-Bers collision occurs, then the flow is absolutely unstable. Such pinching processes are very effective in determining AI/CI in a fluid flow, but they require heavy computations to obtain the spatial branches $k_n(\omega)$. For the inertialess instability of the two-layer film flow down an inclined plate, an illustration of the deformation of the spatial branches $k_n(\omega)$ for decreasing growth rates ω_i from 0.03 to −0.01 is shown in Fig. 5 for $m=2.5$, $\gamma=1$, $\delta=1$, and $\theta=0.2$. Obviously from this figure, no collision occurs under the pinching process, and the flow is then identified to be con-

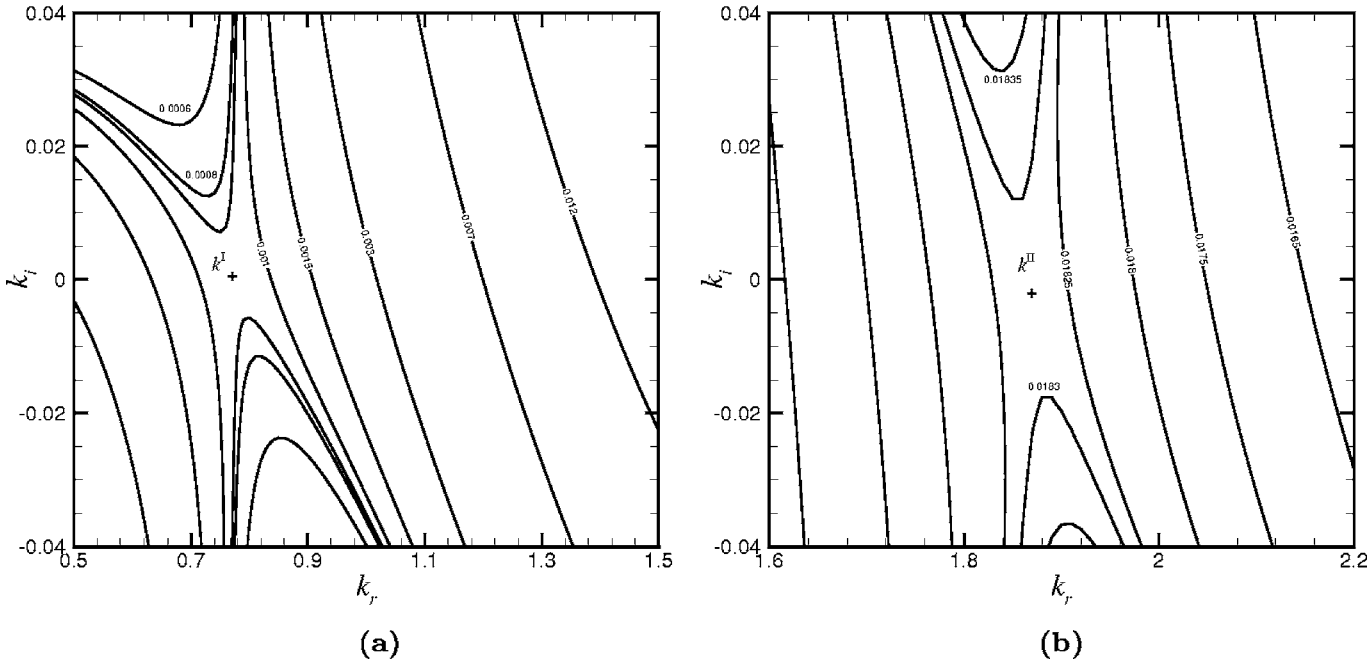

FIG. 6. Saddle points satisfying the Briggs-Bers collision criterion in different moving reference frames for $m=2.5$, $\gamma=1$, $\delta=1$, and $\theta=0.2$: (a) $V=1.18$ and $k^{I}=(0.77,0.00064)$ with $\omega^{\mathrm{I}}=(-0.061,0.00087)$, (b) $V=1.282$ and $k^{\mathrm{II}}=(1.87,-0.0018)$ with $\omega^{\mathrm{II}}=(-0.162,0.0183)$.

vectively unstable. By performing the pinching process for other values of the characteristic parameters m and γ with the same incline angle $\theta=0.2$, the two-layer fluid flow is still found to be convectively unstable.

In order to clearly define the characteristics of the convectively unstable two-layer flow, it is necessary to study the response of the flow to a localized disturbance along an arbitrary fixed spatio-temporal ray, $V=x/t$, as $t\to\infty$. This is equivalent to analyzing how the response evolves in a reference frame moving at the velocity V. If we introduce the Doppler-shifted frequency $\omega^{v}=\omega-Vk$ and use $k^{v}=k$, the dispersion relation in the moving coordinate system will be

$$D_v(k^v,\omega^v)=D(k^v,\omega^v+Vk^v)=0. \tag{4.1}$$

Due to $d\omega^v/dk^v=0$, the saddle point k^* will take place at

$$D(k^*,\omega^*)=0 \quad \text{and} \quad \frac{d\omega}{dk}(k^*,\omega^*)=V, \tag{4.2}$$

and then the absolute growth rate in the moving frame is obtained at $k_0^v=k^*$ through

$$\omega_0^v=\omega^*-Vk^*. \tag{4.3}$$

Here also, the saddle point k^* obtained from (4.2) must verify the Briggs-Bers collision criterion mentioned above.

For $V=1.18$ and $V=1.282$, as shown in Fig. 6, saddle points have been found which are both near the real k axis. In fact, as you will see later (Fig. 7), the growth rate for $V=1.18$ is near the local minimum growth rate while for $V=1.282$ it is near the local maximum growth rate. Obviously, these points are both pinch points produced by a collision of two spatial branches coming from opposite sides of the real k axis.

From these two saddle points and by varying the ray velocity V, it has been possible to determine branches of saddle points by continuation with the use of an iteration method (cf. Deissler[15] and Yin *et al.*[16]). The two branches thus obtained are shown in Fig. 7 through the plots of the growth rate ω_i^v, the oscillatory frequency ω_r^v, the local spatial amplification rate $-k_i^v$, and the local spatial wave number k_r^v as a function of the ray velocity V. The branch in the left-hand side of the graphs corresponds to the long wave instability (let us denote it "branch I"); the other branch corresponds to the short wave instability and will be referred to as "branch II." The short wave instability has the faster downstream velocity, and its maximum growth rate occurs near $V=1.28$. The long wave instability has a slower downstream velocity, but also a far smaller maximum growth rate. When $V=1.21877$, the two curves giving the variation of the growth rate for the two branches intersect, indicating a possible transition between long wave and short wave instability. This phenomenon is different from what was observed in the temporal instability analysis as the growth rates were there continuously varying from the long wave to the short wave region. To confirm this transition, it is necessary to determine which one of these two modes is the dominant mode of instability in the vicinity of the intersection point; this can also be done by using the Briggs-Bers collision criterion.

We have then performed two pinching processes for $V=1.2195$ and $V=1.218$, slightly above and below the value of V at the intersection point (Figs. 8 and 9). For $V=1.2195$ (Fig. 8), it is found that a Briggs-Bers collision occurs at finite wave number $[k^{\mathrm{II}}=(3.55,-0.6)]$ when decreasing the growth rate from $\omega_i=0.00225$ to $\omega_i=0.002178$. Then, when decreasing the growth rate from $\omega_i=0.002178$ to $\omega_i=0.001767$, another collision occurs, but now the saddle point (found at smaller wave number) does not satisfy the Briggs-Bers collision criterion. From these collision analy-

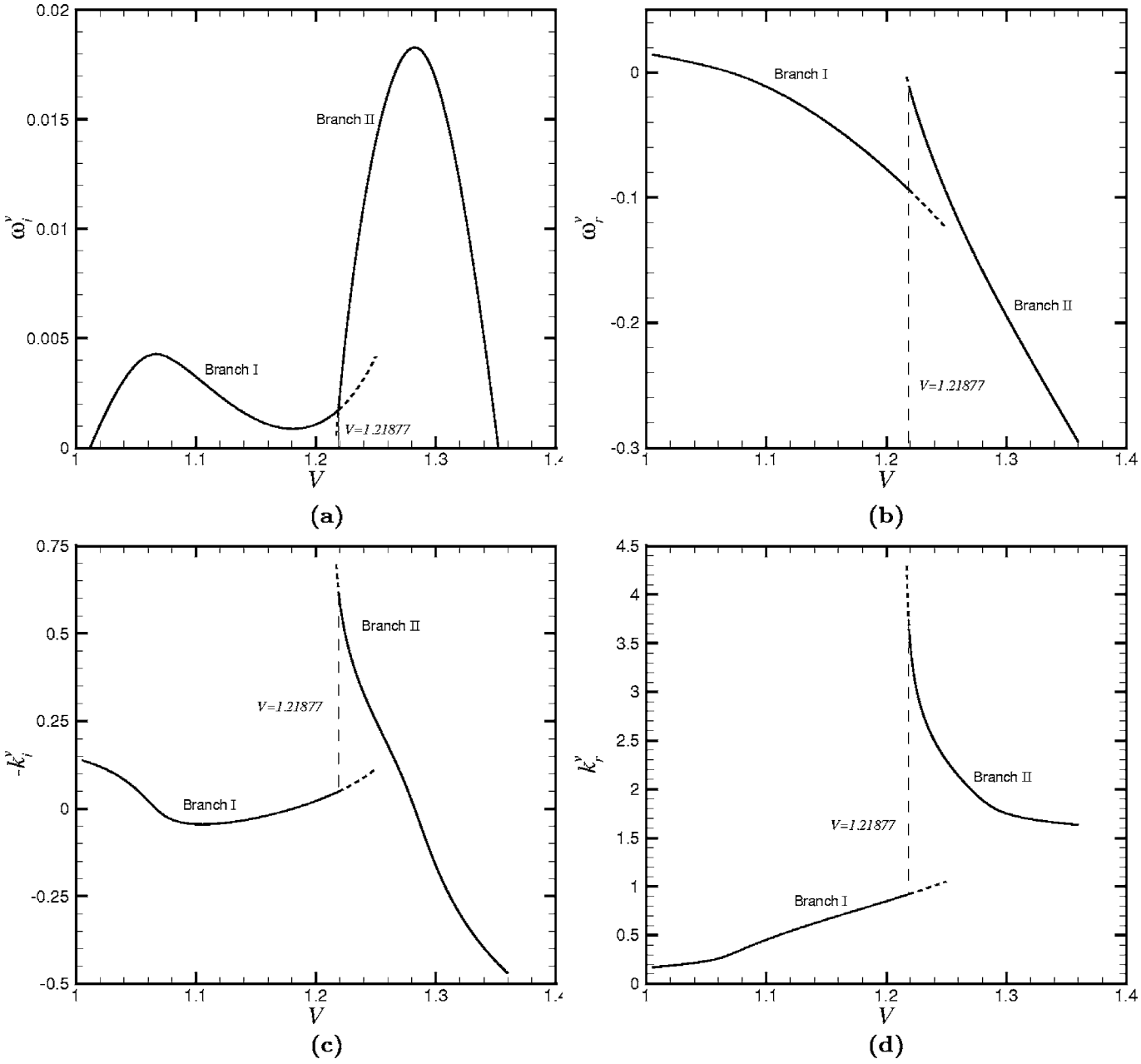

FIG. 7. (a) Growth rate ω_i^v, (b) oscillatory frequency ω_r^v, (c) local spatial amplification rate $-k_i^v$, and (d) local spatial wave number k_r^v as a function of the ray velocity V, for $m=2.5$, $\gamma=1$, $\delta=1$, and $\theta=0.2$.

ses, we can understand that branch II dominates the spatio-temporal growth when $V>1.21877$, i.e., when the moving frame velocity is larger than that of the intersection point. For $V=1.218$ (Fig. 9), through a similar analysis, it is found that a Briggs-Bers collision occurs at small wave number $[k^{\mathrm{I}}=(0.918,-0.048)]$, while a non-Briggs-Bers collision occurs at finite wave number $[k^{\mathrm{II}}=(3.87,-0.65)]$, which shows that the spatio-temporal growth is dominated by branch I when $V<1.21877$. Considering again Fig. 7(a), we can conclude that the Briggs-Bers collision criterion is verified at the saddle-points corresponding to the parts of the branches which have the larger growth rate. The intersection point at $V=1.21877$ is then a real transition point which can be used to distinguish the long wave and short wave instabilities for inertialess two-layer film flow. Furthermore, as can be seen clearly in Figs. 7(b)–7(d), the oscillatory frequency, local spatial amplification rate, and local spatial wave number are found to jump from branch I to branch II at this transition point, which indicates a discontinuity for these quantities.

Finally, we study the evolution of the growth rate ω_i^v of the spatio-temporal instability as a function of the ray velocity V for different density ratios and different viscous ratios (Fig. 10). The two figures confirm what was found in the temporal analysis about the influence of the density and viscous ratios on the inertialess instability, i.e. principally, that the larger is the density ratio, the more unstable is the two-layer system, and that the maximum growth rate occurs at moderate viscous ratio. We also find that when $m=4.0$ and $\gamma=1.0$, the two branches do not intersect anymore in the unstable region.

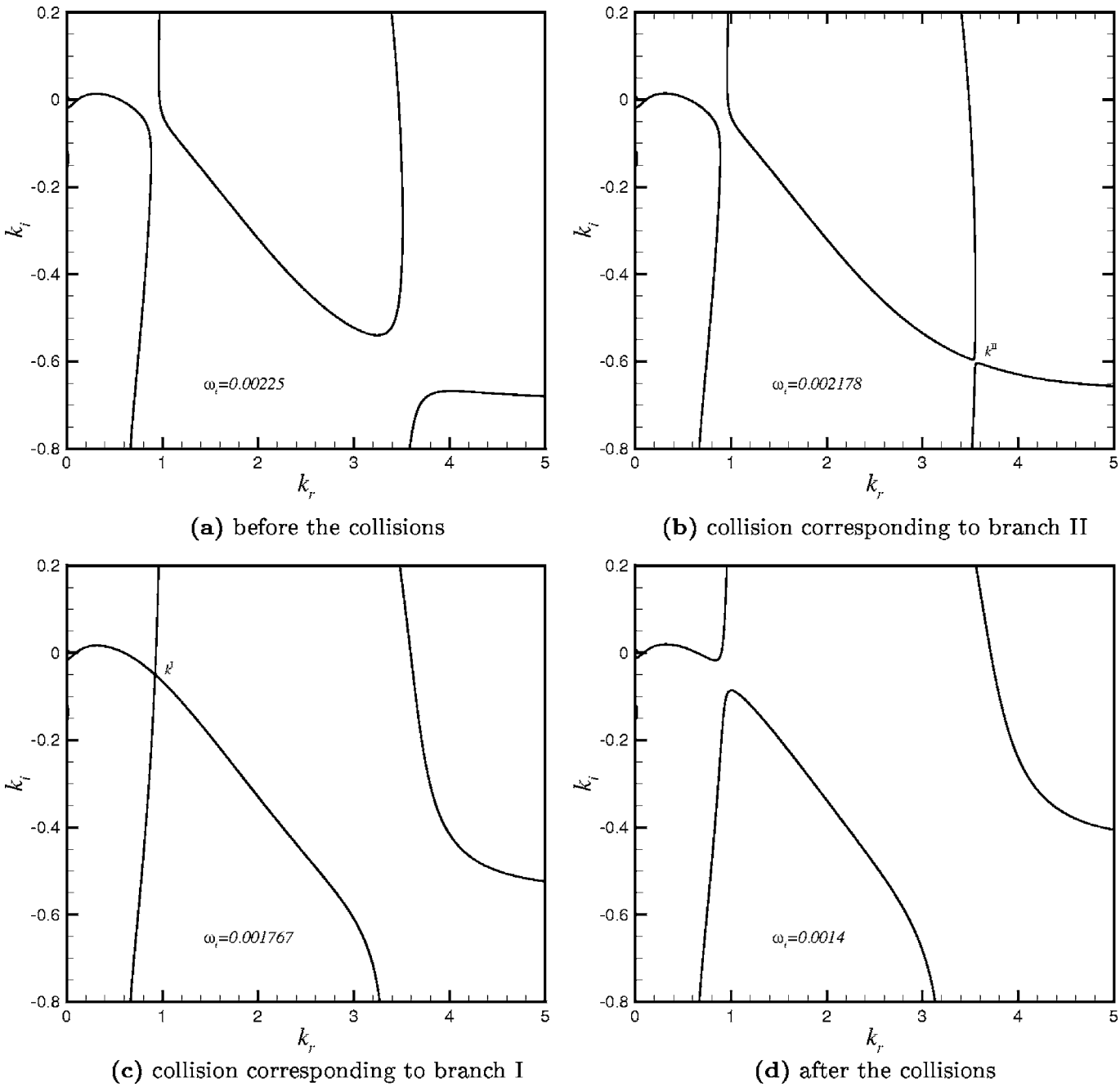

FIG. 8. Pinching process in the complex wave number plane (k_r,k_i) for $V=1.2195$, $m=2.5$, $\gamma=1$, $\delta=1$, and $\theta=0.2$.

V. ABSOLUTE/CONVECTIVE INSTABILITY TRANSITION

Due to the presence of the absolute Rayleigh-Taylor instability for $\theta=0$, it can be expected that the inertialess instability due to the interface will become absolutely unstable when the incline angle approaches zero and the upper layer has the higher density. For $\theta=0.2$, the flow was found to be convectively unstable for usual values of the parameters such as density, depth, and viscosity ratios. But for smaller incline angles, the transition from convective to absolute instability was effectively detected. The boundary curves corresponding to this transition are plotted in Figs. 11 for different values of the parameters.

Figures 11 globally show that the smaller the incline angle, the more easily the system will become absolutely unstable. Figure 11(a) which plots the boundary curves $\delta-\gamma$ for different small incline angles and $m=2.5$, shows that there is a minimum for the critical density ratio; this minimum occurs at a moderate depth ratio near 0.9. Figures 11(b) and 11(c) show boundary curves for equal depth ratio ($\delta=1.0$), Fig. 11(b) giving $m-\gamma$ curves for different values of θ, and Fig. 11(c) giving $\theta-\gamma$ curves for different values of m. These two figures indicate that the smaller the viscosity ratio, the smaller the density ratio needed for the transition. Finally from Fig. 11(c), it is found that when decreasing the incline angle, the critical density ratio approaches 1, in

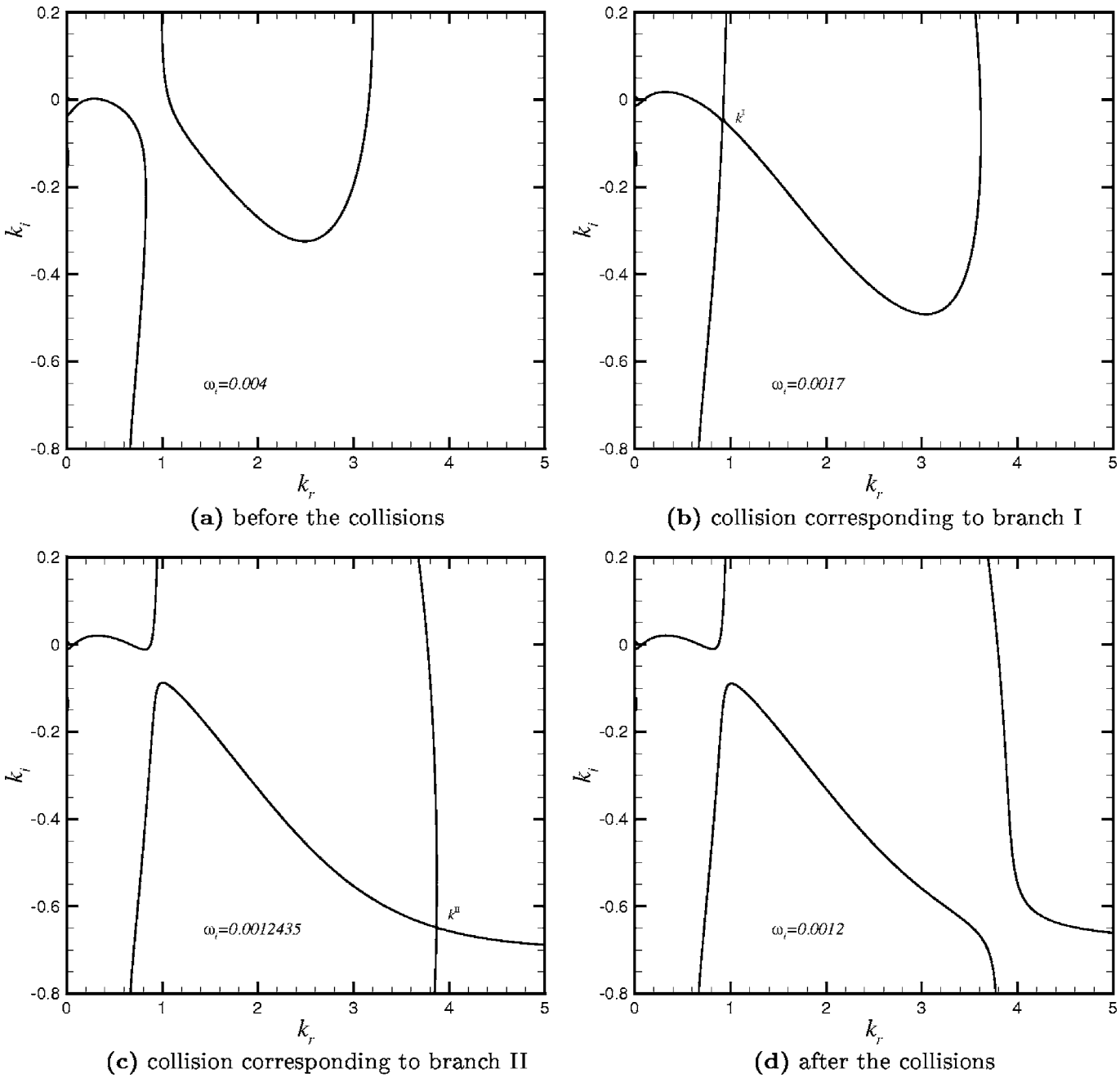

FIG. 9. Pinching process in the complex wave number plane (k_r,k_i) for $V=1.218$, $m=2.5$, $\gamma=1$, $\delta=1$, and $\theta=0.2$.

agreement with the Rayleigh-Taylor instability at $\theta=0$. Moreover, when increasing the density ratio, the incline angle on the boundary curve seems to approach an asymptotic value which is dependent on the viscosity ratio.

VI. SPATIALLY AMPLIFYING WAVES

As Brevdo *et al.*[9] pointed out for a single layer film flow, spatially amplifying linear waves can be generated in a convectively unstable flow by applying a spatially localized harmonic forcing with small amplitude. In fact, the response to a periodic forcing usually referred to as a signaling problem is determined by a spatial instability analysis which can be formulated as

$$D(k,\omega_r)=0. \tag{6.1}$$

For the computation of spatial growth rates, Gaster[17] proved that there exists a relation between the spatial and the temporal growth rates when they are both small,

$$-k_i(S)=\frac{\omega_i(T)}{\partial\omega_r/\partial k_r}, \tag{6.2}$$

where S and T indicate that the values have been computed from spatial and temporal analyses, respectively. In Table I, we first compare the spatial growth rates computed by Gaster transformation to those obtained by direct computation with an iteration method. It can be seen that when the density ratio increases, the spatial growth rate increases too, but the

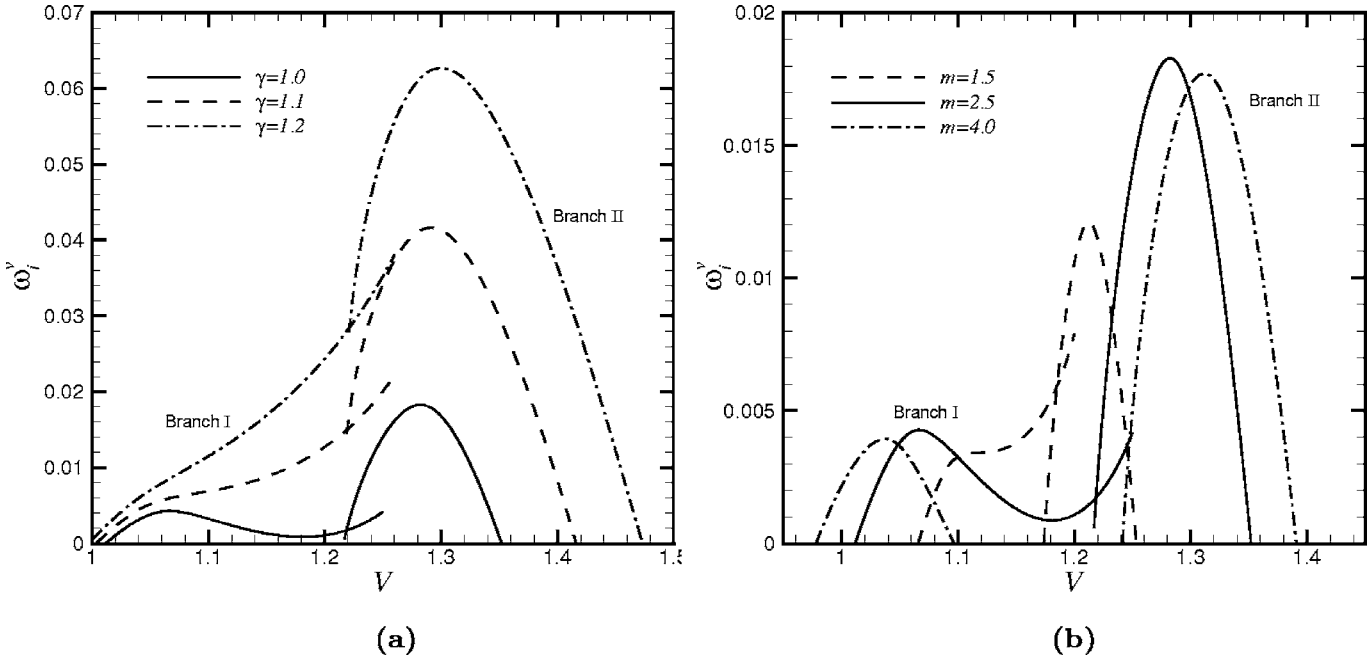

FIG. 10. Growth rate ω_i^v as a function of the ray velocity V for (a) $m=2.5$ and different density ratios, and (b) $\gamma=1.0$ and different viscous ratios ($\delta=1$ and $\theta=0.2$).

corresponding relative error between the results obtained by Gaster transformation and by direct computation also becomes larger. For the smallest value of $\omega_i(\mathrm{T})(\gamma=1.5)$, the relative error is quite small and a good estimation of $-k_i(S)$ is then obtained through the Gaster transformation, confirming the indications of Gaster.[17]

Since the direct computation with an iteration method does not consume too much computer time, we choose this more accurate method to compute the spatial growth rates $-k_i$ and spatial wave numbers k_r as a function of the forcing frequency ω_r for different density ratios and different viscous ratios. The results for $-k_i$ are shown in Fig. 12. By comparing Fig. 12(a) to Fig. 3(a) and Fig. 12(b) to Fig. 3(b), we see that the response obtained in the spatial instability analysis in terms of the spatial growth rate $-k_i$ is similar to that obtained in the temporal instability analysis in terms of the temporal growth rate ω_i. Therefore, here again, increasing the density ratio results in an increase of the growth rate, and the maximum spatial growth rate reaches a maximum at moderate viscous ratio. Due to the nonconsideration of the surface tensions at both the free surface and the interface, an unstable spatial growth rate still exists at very high forcing frequency, which corresponds to the unstable temporal growth rate existing at large wave number (or short wavelength). Note that, as identified by Chen,[7] surface tension effects are likely to stabilize these high frequency and large wave number disturbances. Concerning the spatial wave number k_r, it has been found to increase almost linearly with the forcing frequency.

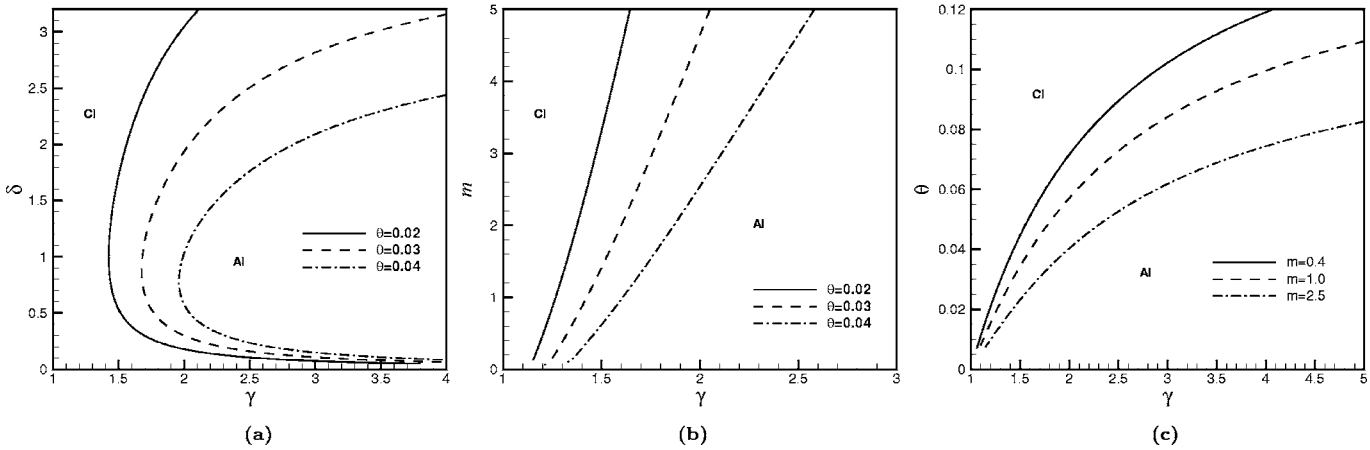

FIG. 11. Boundary curves between absolute and convective instability: (a) $\delta-\gamma$ curves for $m=2.5$ and different incline angles, (b) $m-\gamma$ curves for $\delta=1.0$ and different incline angles, and (c) $\theta-\gamma$ curves for $\delta=1.0$ and different viscosity ratios.

TABLE I. Comparison between Gaster transformation and direct computation with iteration method for spatial growth rates, when $k_r=1.8$, $m=2.5$, $\delta=1.0$, and $\theta=0.2$.

Density ratios	Gaster transformation			Direct computation with iteration method		Relative error for $-k_i$
	ω_i (T)	ω_r	$-k_i$	ω_r	$-k_i$	err(%)
$\gamma=1.5$	0.1148922	2.116529	0.08680595	2.117028	0.08717808	0.43
$\gamma=2.0$	0.1765106	2.101721	0.13115296	2.101796	0.13225215	0.83
$\gamma=4.0$	0.2903197	2.078259	0.20980954	2.074838	0.21361655	1.78

VII. CONCLUSION

The paper presents a thorough analysis of the inertialess linear interfacial instability of two-layer film flows down an incline. The value of the incline angle is generally taken as $\theta=0.2$ and no surface tension is accounted for.

Following the work of Loewenherz and Lawrence,[2] the temporal stability problem is reduced to a linear system of algebraic equations, and solved by the determinants method. The density stratification influence, combined with that of viscosity stratification, is systematically investigated, in contrast with the work of Loewenherz and Lawrence[2] which was restricted to the role of viscosity stratification.

As expected, when the heavier fluid is above ($\gamma>1$), the flow is always unstable. Increasing the density ratio then has a destabilizing effect. However a stabilizing effect on the long wave instability is found very locally when viscosities in the two layers have nearly the same value [Fig. 2(a)]. Finally, the dominant instability is a short wave instability and its maximum growth rates occur at moderate values of the viscosity ratio (around 2).

When the lighter fluid is above ($\gamma<1$), decreasing the density ratio from 1 has more subtle effects. If the general effect seems stabilizing as the unstable domain in the $m-k$ parameter space rather shrinks, a local destabilization is found for viscosity ratios m slightly less than 1, which increases the range of values where instability is triggered. Another effect is also to select the long wave instability to the detriment of the finite wavelength instability. A threshold value of the density ratio is indeed put in evidence, under which the finite wavelength instability vanishes, however high is the value of the viscosity ratio. The value of this critical density ratio varies from 0.81 in the case of a very thin upper layer to nearly 1 as soon as the upper layer thickness is of the order of 3 times (or more) that of the lower layer (Fig. 4). Finally, it is shown that here also the maximum growth-rate occurs at moderate values of the viscosity ratio.

The spatio-temporal linear stability analysis shows that for $\theta=0.2$, when the flow has been found unstable (i.e., in a wide range of density and viscosity ratios), it is convectively unstable. The paper also provides a study of spatially amplifying waves (Fig. 12), which exhibits similar trends as the results of the temporal analysis; increasing the density ratio results in an increase in growth-rates, and a maximum in

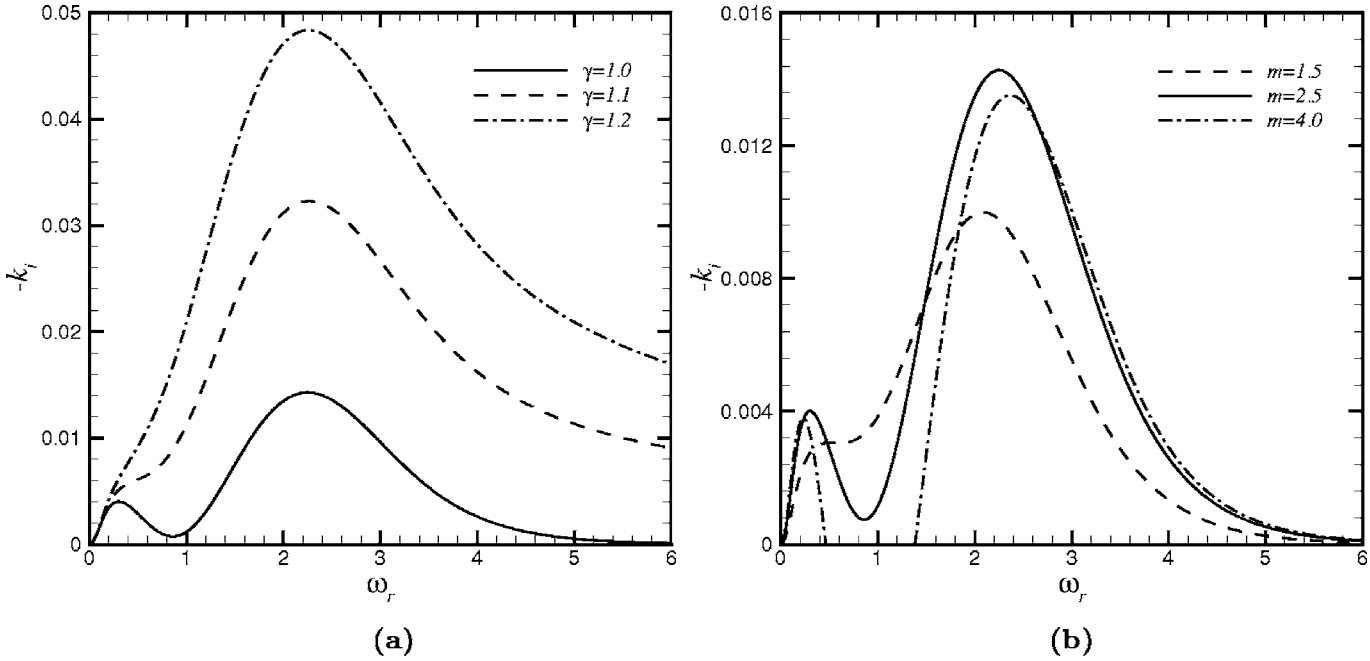

FIG. 12. Spatial growth rate $-k_i$ as a function of the forcing frequency ω_r for (a) $m=2.5$ and different density ratios, and (b) $\gamma=1.0$ and different viscous ratios ($\delta=1$ and $\theta=0.2$).

growth-rates is reached at moderate values of viscosity ratio. It is also found that short waves have larger downstream velocities. More importantly, there is a transition point for the growth-rates as a function of the ray velocity V, which corresponds to a jump in local oscillatory frequency, spatial amplification rate, and spatial wave number. This transition can also be used to distinguish the regions of long wave and short wave instabilities.

Finally, due to the existence of the absolute Rayleigh-Taylor instability for $\theta=0$, the transition from convective to absolute instability has been obtained for small values of θ. The AI/CI boundary curves show that smaller viscous ratios make the flow absolutely unstable at smaller density ratio, and that the minimum critical density ratio occurs at moderate depth ratios.

ACKNOWLEDGMENTS

This work was funded by a fellowship from the Région Rhône-Alpes (J. H.).

APPENDIX

Coefficients α, β, and χ in (2.11),

$$\alpha = \begin{vmatrix} 2k^2e^{-k\delta} & 2k^2e^{k\delta} & 2(k-\delta k^2)e^{-k\delta} & -2(k+\delta k^2)e^{k\delta} & 0 & 0 & 0 & 0 \\ -2mk^3e^{-k\delta} & 2mk^3e^{k\delta} & 2m\delta k^3e^{-k\delta} & -2m\delta k^3e^{k\delta} & 0 & 0 & 0 & 0 \\ 1 & 1 & 0 & 0 & -1 & -1 & 0 & 0 \\ k & -k & 1 & 1 & -k & k & -1 & -1 \\ 2mk^2 & 2mk^2 & 2mk & -2mk & -2k^2 & -2k^2 & -2k & 2k \\ -2mk^3 & 2mk^3 & 0 & 0 & 2k^3 & -2k^3 & 0 & 0 \\ 0 & 0 & 0 & 0 & e^k & e^{-k} & e^k & e^{-k} \\ 0 & 0 & 0 & 0 & ke^k & -ke^{-k} & (1+k)e^k & (1-k)e^{-k} \end{vmatrix},$$

$$\beta = i(a+b),$$

$$a = \begin{vmatrix} 0 & 2k^2e^{-k\delta} & 2k^2e^{k\delta} & 2(k-\delta k^2)e^{-k\delta} & -2(k+\delta k^2)e^{k\delta} & 0 & 0 & 0 & 0 \\ 0 & -2mk^3e^{-k\delta} & 2mk^3e^{k\delta} & 2m\delta k^3e^{-k\delta} & -2m\delta k^3e^{k\delta} & 0 & 0 & 0 & 0 \\ 0 & 1 & 1 & 0 & 0 & -1 & -1 & 0 & 0 \\ ik[DU_2(0)-DU_1(0)] & k & -k & 1 & 1 & -k & k & -1 & -1 \\ iU_2(0)k & 0 & 0 & 0 & 0 & -1 & -1 & 0 & 0 \\ i[D^2U_2(0)-mD^2U_1(0)]k & 2mk^2 & 2mk^2 & 2mk & -2mk & -2k^2 & -2k^2 & -2k & 2k \\ (\gamma-1)K\cot\theta k^2 & -2mk^3 & 2mk^3 & 0 & 0 & 2k^3 & -2k^3 & 0 & 0 \\ 0 & 0 & 0 & 0 & 0 & e^k & e^{-k} & e^k & e^{-k} \\ 0 & 0 & 0 & 0 & 0 & ke^k & -ke^{-k} & (1+k)e^k & (1-k)e^{-k} \end{vmatrix},$$

$$b = \begin{vmatrix} iU_1(-\delta)k & -e^{-k\delta} & -e^{k\delta} & \delta e^{-k\delta} & \delta e^{k\delta} & 0 & 0 & 0 & 0 \\ -iD^2U_1(-\delta)k & 2k^2e^{-k\delta} & 2k^2e^{k\delta} & 2(k-\delta k^2)e^{-k\delta} & -2(k+\delta k^2)e^{k\delta} & 0 & 0 & 0 & 0 \\ \gamma K\cot\theta k^2 & -2mk^3e^{-k\delta} & 2mk^3e^{k\delta} & 2m\delta k^3e^{-k\delta} & -2m\delta k^3e^{k\delta} & 0 & 0 & 0 & 0 \\ 0 & 1 & 1 & 0 & 0 & -1 & -1 & 0 & 0 \\ 0 & k & -k & 1 & 1 & -k & k & -1 & -1 \\ 0 & 2mk^2 & 2mk^2 & 2mk & -2mk & -2k^2 & -2k^2 & -2k & 2k \\ 0 & -2mk^3 & 2mk^3 & 0 & 0 & 2k^3 & -2k^3 & 0 & 0 \\ 0 & 0 & 0 & 0 & 0 & e^k & e^{-k} & e^k & e^{-k} \\ 0 & 0 & 0 & 0 & 0 & ke^k & -ke^{-k} & (1+k)e^k & (1-k)e^{-k} \end{vmatrix},$$

$$\chi = - \begin{vmatrix} iU_1(-\delta)k & 0 & -e^{-k\delta} & -e^{k\delta} & \delta e^{-k\delta} & \delta e^{k\delta} & 0 & 0 & 0 & 0 \\ -iD^2U_1(-\delta)k & 0 & 2k^2e^{-k\delta} & 2k^2e^{k\delta} & 2(k-\delta k^2)e^{-k\delta} & -2(k+\delta k^2)e^{k\delta} & 0 & 0 & 0 & 0 \\ \gamma K\cot\theta k^2 & 0 & -2mk^3e^{-k\delta} & 2mk^3e^{k\delta} & 2m\delta k^3e^{-k\delta} & -2m\delta k^3e^{k\delta} & 0 & 0 & 0 & 0 \\ 0 & 0 & 1 & 1 & 0 & 0 & -1 & -1 & 0 & 0 \\ 0 & ik[DU_2(0)-DU_1(0)] & k & -k & 1 & 1 & -k & k & -1 & -1 \\ 0 & iU_2(0)k & 0 & 0 & 0 & 0 & -1 & -1 & 0 & 0 \\ 0 & i[D^2U_2(0)-mD^2U_1(0)]k & 2mk^2 & 2mk^2 & 2mk & -2mk & -2k^2 & -2k^2 & -2k & 2k \\ 0 & (\gamma-1)K\cot\theta k^2 & -2mk^3 & 2mk^3 & 0 & 0 & 2k^3 & -2k^3 & 0 & 0 \\ 0 & 0 & 0 & 0 & 0 & 0 & e^k & e^{-k} & e^k & e^{-k} \\ 0 & 0 & 0 & 0 & 0 & 0 & ke^k & -ke^{-k} & (1+k)e^k & (1-k)e^{-k} \end{vmatrix},$$

where $||$ represents the determinant of the corresponding matrix.

[1] H.-C. Chang, "Wave evolution on a falling film," Annu. Rev. Fluid Mech. **26**, 103 (1994).

[2] D. S. Loewenherz and C. J. Lawrence, "The effect of viscosity stratification on the instability of a free surface flow at low Reynolds number," Phys. Fluids A **1**, 1686 (1989).

[3] T. W. Kao, "Stability of two-layer viscous stratified flow down an inclined plane," Phys. Fluids **8**, 812 (1965).

[4] T. W. Kao, "Role of the interface in the stability of stratified flow down an inclined plane," Phys. Fluids **8**, 2190 (1965).

[5] T. W. Kao, "Role of viscosity stratification in the instability of two-layer flow down in incline," J. Fluid Mech. **33**, 561 (1968).

[6] C. S. Yih, "Stability of liquid flow down an inclined plane," Phys. Fluids **6**, 321 (1963).

[7] K. P. Chen, "Wave formation in the gravity-driven low-Reynolds number flow of two liquid films down an inclined plane," Phys. Fluids A **5**, 3038 (1993).

[8] W. Y. Jiang, B. Helenbrook, and S. P. Lin, "Inertialess instability of a two-layer liquid film flow," Phys. Fluids **16**, 652 (2004).

[9] L. Brevdo, P. Laure, F. Dias, and T. J. Bridges, "Linear pulse structure and signaling in a film flow on an inclined plane," J. Fluid Mech. **396**, 37 (1999).

[10] J. Liu, J. D. Paul, and J. P. Gollub, "Measurements of the primary instabilities of film flows," J. Fluid Mech. **250**, 69 (1993).

[11] R. J. Briggs, *Electron-Stream Interaction with Plasmas* (MIT Press, Cambridge, 1964).

[12] A. Bers, "Theory of absolute and convective instabilities," in Survey Lectures, *Proceedings of the International Congress on Waves and Instabilities in Plasmas*, edited by G. Auer and F. Cap (Institute for Theoretical Physics, Innsbruck, 1973), p. B1.

[13] P. Huerre and P. A. Monkewitz, "Absolute and convective instabilities in free shear layers," J. Fluid Mech. **159**, 151 (1985).

[14] P. Huerre and P. A. Monkewitz, "Local and global instabilities in spatially developing flows," Annu. Rev. Fluid Mech. **22**, 473 (1990).

[15] R. J. Deissler, "Spatially growing waves, intermittency, and convective chaos in an open-flow system," Physica D **25**, 233 (1987).

[16] X. Y. Yin, D. J. Sun, M. J. Wei, and J. Z. Wu, "Absolute and convective instability character of slender viscous vortices," Phys. Fluids **12**, 1062 (2000).

[17] M. Gaster, "A note on the relation between temporally-increasing and spatially-increasing disturbances in hydrodynamic stability," J. Fluid Mech. **14**, 222 (1962).